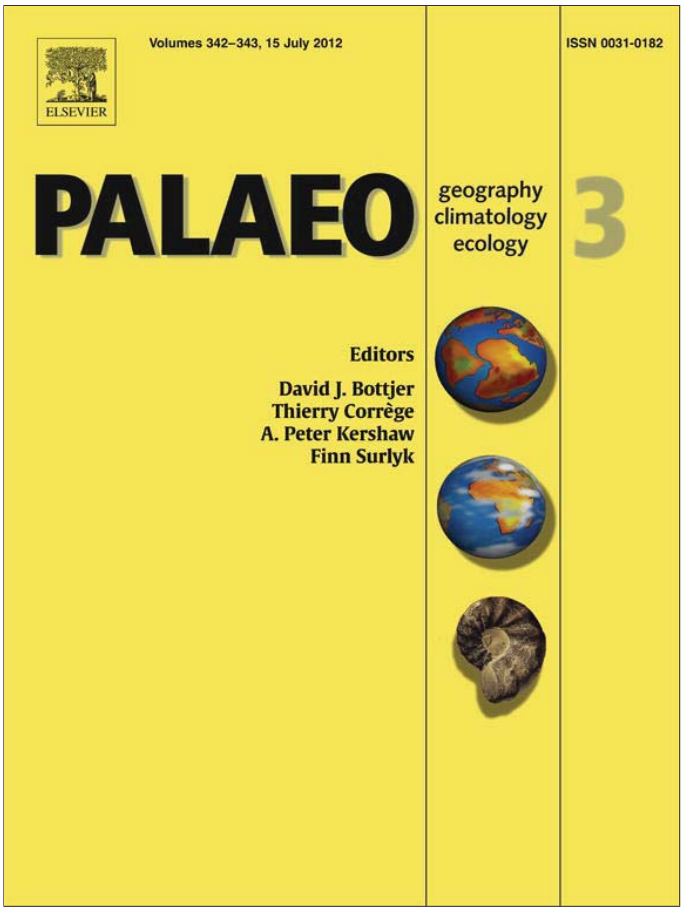

Palaeogeography, Palaeoclimatology, Palaeoecology 342–343 (2012) 17–26

Contents lists available at SciVerse ScienceDirect

Palaeogeography, Palaeoclimatology, Palaeoecology

journal homepage: www.elsevier.com/locate/palaeo

Increased continental weathering flux during orbital-scale sea-level highstands: Evidence from Nd and O isotope trends in Middle Pennsylvanian cyclic carbonates

Bethany P. Theiling [a,b,*], Maya Elrick [a], Yemane Asmerom [a]

[a] University of New Mexico, United States
[b] Purdue University, United States

ARTICLE INFO

Article history:
Received 16 September 2011
Received in revised form 16 April 2012
Accepted 18 April 2012
Available online 11 May 2012

Keywords:
Cycles
Orbital-scale
Neodymium
Oxygen
Sea-level
Glacio-eustasy
Continental weathering
$\delta^{18}O$
ε_{Nd}
Glacial–interglacial

ABSTRACT

Despite the common occurrence of orbital-scale (10^4–10^5 yr) sedimentary cycles in a wide range of Proterozoic through Neogene marine and non-marine depositional systems, understanding the effects and phase relationships of orbital-scale climate drivers on time-equivalent marine and non-marine deposits is difficult mainly due to correlation limitations between the geographically isolated deposition settings. Results from this study assess the relationships between orbital-scale continental weathering flux and glacial–interglacial marine cycles using Nd isotopes (from whole rock limestones) and $\delta^{18}O$ values (from conodont apatite) from Middle Pennsylvanian cyclic marine carbonates in the U.S. Southwest.

Conodont $\delta^{18}O$ trends from 2 of 4 sampled glacial–interglacial carbonate cycles support previous interpretations that observed water-depth changes were controlled by glacio-eustasy (30–50 m magnitudes) combined with <1° seawater temperature changes. Two additional sampled cycles show initially increasing, then decreasing $\delta^{18}O$ trends. Based on these results, we suggest that $\delta^{18}O$ better defines a eustatic sea-level curve, rather than a facies-derived curve.

ε_{Nd} trends in 5 of 8 sampled cycles are higher during regressive intervals (early glacial phase) and lower during sea-level highstands (interglacial phase), supporting the hypothesis that increases in precipitation and/or air temperatures during interglacial intervals result in increased continental weathering rates and/or increased flux of weathered solutes to the Middle Pennsylvanian marine basin. This hypothesis is in contrast to traditional sequence stratigraphic interpretations (increased siliciclastic shedding into marine basins during falling sea level/lowstands) and suggests that climatically-controlled precipitation and/or air temperature fluctuations influenced continental weathering flux more than sea level-controlled shoreline or baseline position in this paleotropical location. These results highlight the use of combined ε_{Nd} and $\delta^{18}O$ analyses as a tool for evaluating the response of marine and coeval non-marine systems to orbital-scale climate changes, particularly in deep-time depositional systems.

1. Introduction

Sedimentary cycles (or parasequences) recording orbitally-driven climate changes are documented in a wide range of Precambrian through Phanerozoic marine and continental deposits including shelf, slope, and open-ocean marine environments and fluvial, lacustrine, and paleosol deposits (e.g. Anderson, 1982; Arthur et al., 1986; Goldhammer, 1987; Olson and Kent, 1999; Gale et al., 2002; Laurin et al., 2005; Culver et al., 2011). The widespread occurrence of such cycles across a range of geologic time periods and settings suggests that orbitally-forced climate changes are a major driver of sedimentation patterns at 10^4–10^5 yr timescales.

Despite the common occurrence of orbital cycles in the sedimentary record, it has been difficult to assess the effects and phase relationships of orbital forcing on time-equivalent marine and non-marine deposits, particularly in deep-time systems (pre-Cenozoic). These difficulties are due mainly to limitations related to correlating between marine and geographically isolated non-marine successions at the orbital and sub-orbital timescales using conventional correlation tools such as biostratigraphy, magnetostratigraphy, carbon-isotope stratigraphy, and/or tephrachronology (e.g., Shishkin and Ochev, 1993; Lozovsky and Yarshenko, 1994; Arens and Jahren, 2000; Jahren et al., 2001; Mundil et al., 2003). An additional complexity is that many deep-time marine successions lack coeval continental deposits due to erosion, nondeposition, and/or later deformation. Understanding the flux and timing of continental material (solid and dissolved load) to adjacent marine basins in the context of orbitally-driven climate changes has important implications for evaluating global oceanic elemental and nutrient budgets, biologic productivity, carbon cycling, and pCO_2, with its associated climatic effects.

Some previous attempts to understand the effects of and relationships between orbital-scale climate change and deep-time marine

* Corresponding author at: Purdue University, United States.
E-mail address: btheilin@purdue.edu (B.P. Theiling).

0031-0182/$ – see front matter © 2012 Elsevier B.V. All rights reserved.
doi:10.1016/j.palaeo.2012.04.017

and coeval continental deposits were conducted on interbedded marine and non-marine facies (Soreghan, 1994; Miller et al., 1996; Rankey, 1997). Continental climate interpretations were based on the nature and occurrence of climatically sensitive non-marine facies (i.e., eolian, paleosols, fluvial deposits), whereas sea-level interpretations tracking glacial–interglacial climate phases and glacio-eustasy were made from interbedded cyclic marine deposits. Soreghan (1994) and Rankey (1997) interpreted wetter Pennsylvanian continental climates during interglacial phases (sea-level highstands) with drier conditions during glacial phases (sea-level lowstands). In contrast, Miller et al. (1996), working on Permian deposits, report wetter or more seasonally variable conditions during glacial phases (sea-level lowstands). These opposing interpretations are due in part to the fact that the analyzed successions contained interbedded continental and marine deposits which are not strictly time-equivalent and therefore cannot track coeval climatic responses to orbital forcing.

Alternative approaches to evaluating the effects of orbital climate change in marine and coeval non-marine systems include combined analysis of geochemical proxies for sea surface temperature (SST) and glacio-eustasy ($\delta^{18}O$ values) and continental weathering flux (Os, Sr, and/or Nd isotopes) that occur in marine strata. The use of these proxies within fully marine successions removes potential effects of miscorrelation between marine and non-marine strata and does not require the presence of coeval non-marine successions. Although Sr isotopes have been utilized in a variety of studies to track changes in mantle versus continental flux, the $>10^6$ yr oceanic residence time for Sr precludes its use in orbital-scale paleoclimate studies. The short oceanic residence time of Nd (10^2 yr) however, implies that Nd-isotopic ratios will be incorporated into marine sedimentary deposits before homogenization by oceanic mixing. In addition, REE are immobile (insoluble) and therefore, relatively unsusceptible to diagenesis (McLennan, 1989; Banner, 2004). Therefore, Nd isotopes can be utilized for regional-scale continental weathering flux studies to evaluate orbital- and suborbital-scale climate changes across varying climate zones/belts.

Recent advances in multi-collector inductively coupled mass spectrometry (MC-ICPMS) have made possible the rapid high-precision isotopic analysis of small quantities of Nd, opening the use of Nd isotopic data for high-resolution chemostratigraphic reconstruction in carbonates. The objectives of this study are to describe and interpret changes in $\delta^{18}O$ values from conodont apatite and Nd-isotopes from cyclic whole rock limestones to assess the effects and timing relationships between orbitally driven glacial–interglacial marine cycles and continental weathering flux (a term we use to refer to continental weathering rates and/or transport to a basin).

2. Geologic background

The Pennsylvanian Earth system was dominated by the early formation of the Pangaean supercontinent, the large Panthalassa ocean, and by major fluctuations in continental ice-volume centered in high-latitude Gondwana (Caputo and Crowell, 1985; Veevers and Powell, 1987; Frakes and Francis, 1988; Crowell, 1999; Scotese, 2001; Isbell et al., 2003; Fielding et al., 2008). Growth and melting of glaciers caused sea-level fluctuations of >50 m (e.g. Heckel, 1977; Goldhammer and Elmore, 1984; Soreghan, 1994; Joachimski et al., 2006; Rygel et al., 2008; Elrick et al., 2009) which generated orbital-scale cycles (Heckel, 1977, 1994, 1977; Soreghan and Giles, 1999) and million year (My)-scale depositional sequences (Algeo et al., 1991; Soreghan, 1994; Wiberg and Smith, 1994; Scott and Elrick, 2004; Elrick and Scott, 2010).

During the Pennsylvanian, New Mexico was located approximately 5–10° south of the paleoequator (Scotese and Galonka, 1992). Tectonic subsidence rates related to Ancestral Rocky Mountain deformation were minimal during the Early and Middle Pennsylvanian and highest during the Late Pennsylvanian (Virgillian or Gzhelian) (Dickinson and Lawton, 2003).

The Middle Pennsylvanian (Desmoinesian or Moscovian) Gray Mesa Formation accumulated in the Lucero Basin of central New Mexico (Fig. 1; Kelly and Wood, 1946; Martin, 1971; Kues and Giles, 2004) and comprised nearly 300 m of cyclic, mixed carbonate–siliciclastic marine deposits (Martin, 1971; Scott and Elrick, 2004; Elrick and Scott, 2010). The Lucero Basin was surrounded by relatively low-relief Precambrian crystalline uplifts (~1.4–1.65 Ga; Karlstrom et al., 2004) associated with formation of the Ancestral Rocky Mountains (Fig. 1; Kluth and Coney, 1981; Ye et al., 1996). Within the Lucero Basin, northward increases in both siliciclastic sediment abundance and grain size suggest sourcing from the nearby Penasco Uplift to the northeast (Martin, 1971; Scott and Elrick, 2004). Age control for the Grey Mesa Formation is based on limited fusulinid and conodont biostratigraphy (Kelly and Wood, 1946; Wengerd, 1959; Martin, 1971).

At the Mesa Sarca study area (Fig. 1), the Gray Mesa Formation is composed of ~75 orbital-scale upward-shallowing subtidal cycles (or parasequences) (Scott and Elrick, 2004). Subtidal cycles provide a more continuous record of deposition relative to peritidal cycles because of relatively uninterrupted deposition in subtidal marine environments. Typical Gray Mesa subtidal cycles (1.5–5 m) are characterized by thinly bedded, argillaceous, skeletal mudstone/wackestone or covered intervals at cycle bases (deeper subtidal facies), thin- to medium-bedded, bioturbated skeletal wackestone/packstone in the middle of cycles (shallow subtidal facies), with medium- to thick-bedded, skeletal wackestone/packstone and rare grainstone cycle caps (shallowest subtidal facies). Approximately 40% of cycle caps display evidence of subaerial exposure, including meteoric $\delta^{13}C$ signatures, calcretes, and regolith breccias (Fig. 2; Scott and Elrick, 2004; Elrick and Scott, 2010).

Previous studies of Gray Mesa cycles in the study area document orbital-scale sea-level fluctuations and systematic up-cycle increases in whole rock $\delta^{13}C$ and conodont $\delta^{18}O$, which together indicate that high-amplitude (>50 m) glacio-eustasy was responsible for cycle development and subaerial exposure during sea-level fall/lowstands (Scott and Elrick, 2004; Elrick and Scott, 2010).

3. Methodology

This study focuses on samples collected from 8 successive, subtidal cycles in the lower 35 m of the Gray Mesa Formation (highstand systems tract of Sequence 1; Scott and Elrick, 2004).

3.1. Oxygen isotopes

Analyses of conodont $\delta^{18}O$ were used to verify that Gray Mesa cycles sampled for Nd isotopes formed in response to orbital-scale glacio-eustasy. Oxygen isotopes from marine calcite are a well-established tool for determination of seawater temperature changes and ice-volume effects (e.g. Emiliani, 1966; Epstein et al., 1953; Emiliani, 1955; Shackleton and Opdyke, 1973; Veizer et al., 1999). $\delta^{18}O$ from conodont apatite is considered more reliable for pre-Mesozoic studies than calcite because it is less susceptible to diagenetic alteration (Bryant et al., 1996; Iacumin et al., 1996; Wenzel et al., 2000; Joachimski et al., 2004). Conodont apatite has been shown to precipitate in equilibrium with ambient seawater when compared to coeval fish teeth (Amzy et al., 1998). In addition, conodont $\delta^{18}O$ values demonstrate smaller isotopic variability than coeval calcite (Wenzel et al., 2000).

Samples for conodont analyses were collected at 0.1–0.5 m intervals depending on observed facies changes, with individual samples weighing between 10 and 25 kg. Conodonts were extracted from whole rock limestones using conventional separation techniques of Sweet and Harris (1988).

Oxygen isotopic analyses were performed on ~500 μg of Ag_3PO_4 crystals, formed from the conversion of conodont apatite using a method modified from O'Neil et al. (1994) and Bassett et al. (2007). Isotopic ratios were determined by reducing Ag_3PO_4 in a continuous flow TC–EA and analyzed on a Finnigan Mat 253 mass spectrometer

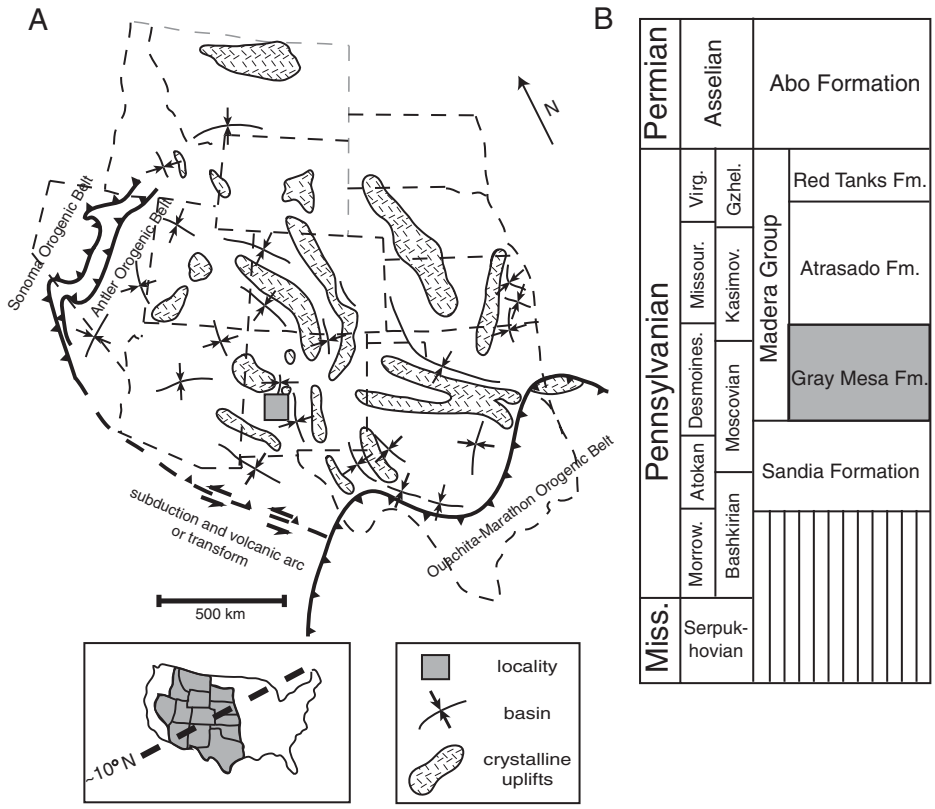

Fig. 1. A) Paleogeographic reconstruction of the western United States showing locations of Precambrian crystalline uplifts, basins, and major faults, with inset showing estimated Pennsylvanian paleolatitude for study area (modified from Kluth and Coney, 1981). Gray shaded square outlines the Lucero Basin and Mesa Sarca study area. B) Pennsylvanian chronostratigraphy of the study area. Abbreviations: Virg. = Virgilian, Missour. = Missourian, Desmoines. = Desmoinesian, Morrow. = Morrowian, Kasimov. = Kasimovian, Gzhel. = Gzhelian.

at the University of New Mexico Stable Isotope Laboratory. Oxygen isotope data are reported in ‰ with respect to SMOW (Table 1). Reproducibility of $\delta^{18}O$ measurements was determined by replicate analyses of internal standards and with an uncertainty of $\pm 0.3‰$ (1σ).

3.2. Neodymium isotopes

^{143}Nd is the decay product of ^{147}Sm ($t_{1/2} = 106$ Ga). Variations in $^{143}Nd/^{144}Nd$ are typically expressed by ε_{Nd} values, defined as $(^{143}Nd/^{144}Nd_{sample}/^{143}Nd/^{144}Nd_{CHUR} - 1) * 10{,}000$, where CHUR is the $^{143}Nd/^{144}Nd$ ratio of the chondritic undifferentiated reservoir at the time of interest. Because Nd has a larger ionic radius than Sm, Nd is considered 'more incompatible' than Sm. More incompatible elements will be preferentially partitioned into the crust during mantle melting and differentiation. Consequently, the continental crust has a lower Sm/Nd ratio than the depleted mantle (as sampled by mid-ocean ridge basalts [MORB]) and as a result, a less radiogenic Nd-isotopic composition (typically $\varepsilon_{Nd} = -20$ for crust with a mean age of 2 Ga; Goldstein and Jacobsen, 1987) compared to MORB (typically $> +8$; Shirey, 1991). The short oceanic residence time of Nd ($< 10^2$ yr) however, implies that Nd-isotopic ratios will be incorporated into marine sedimentary deposits before homogenization by oceanic mixing (oceanic mixing time ~1000 yrs). In addition, REE are immobile (insoluble) and therefore, relatively unsusceptible to diagenesis (McLennan, 1989; Banner, 2004). Therefore, Nd isotopes can be utilized for regional-scale continental weathering flux studies to evaluate orbital- and suborbital-scale climate changes across varying climate zones/belts. Because the seawater REE budget is dominated by continental input (Goldstein and Jacobsen, 1987), ε_{Nd} in marine deposits can serve as a proxy for changes in the regional continental weathering flux, and can be used to track paleo-ocean circulation (e.g. Martin and Macdougall, 1995; Reynolds et al., 1999; Thomas, 2004; Piotrowski et al., 2005; Pucéat et al., 2005; Scher and Martin, 2006; Via and Thomas, 2006; MacLeod et al., 2008) and emergence/flooding of continental landmass (Fanton et al., 2002).

Nd-isotopic analyses were performed on powdered whole-rock limestones collected at a 0.1–1 m sampling resolution. Approximately 500 mg of powder was drilled from each sample using a diamond-bit Dremel© in order to avoid stylolites, intraclasts, large skeletal grains, and veins. The powder was dissolved in 6N HCl. The soluble and insoluble fractions were then centrifuged and the supernate was separated into two Teflon© beakers, one to be used to analyze concentrations of Sm and Nd for calculation of $^{147}Sm/^{144}Nd$, and one to be used for REE and Sm–Nd column separation for analysis of $^{143}Nd/^{144}Nd$.

For this initial effort, we used a small aliquot of the supernate to determine the Sm/Nd ratio of the samples to calculate initial $^{143}Nd/^{144}Nd$ ratios. The Sm/Nd fraction was dried down, dissolved in 200 μL 7N HNO_3, capped, and left overnight. The sample was then dissolved in 50 mL of 10 ppb In + 3% HNO_3, and was analyzed on a Thermo X-series II inductively coupled plasma quadrupole mass spectrometer (ICPQMS) at the University of New Mexico Radiogenic Isotope Laboratory. The initial $^{143}Nd/^{144}Nd$ values were calculated using an age of 300 Ma (approximate depositional age of Gray Mesa Formation; Table 1). We have verified this initial method using a total spiking method, whereby a calibrated spike with known $^{147}Sm/^{150}Nd$ was added to sample supernate to determine sample $^{147}Sm/^{144}Nd$.

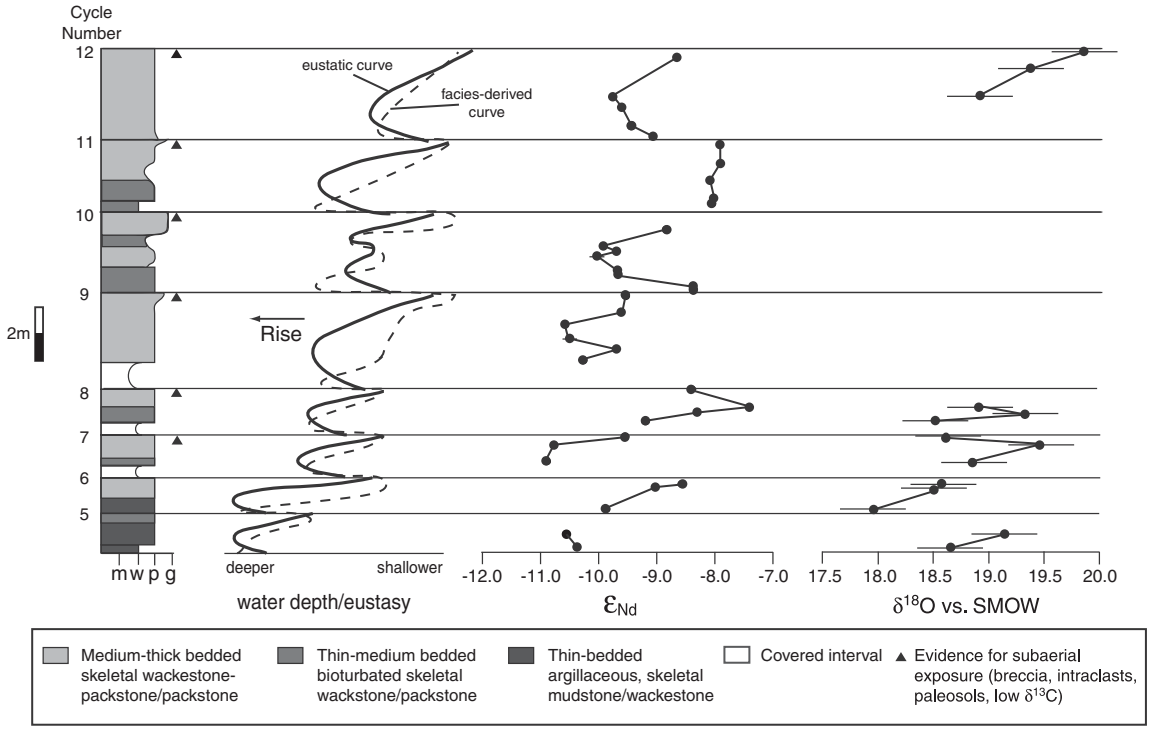

Fig. 2. Cyclostratigraphy of the targeted lower Gray Mesa Formation versus relative water depths (dashed line) determined from facies analysis and eustatic sea-level (solid line) estimated from the combined effects of sedimentation, subsidence, and sea-level change, $\delta^{18}O_{apatite}$, and ε_{Nd} trends. Cycle numbers are based on previous work by Scott and Elrick (2004). $\delta^{18}O$ data from cycle 12 is taken from Elrick and Scott (2010). Error bars for ε_{Nd} are smaller than the size of the data point, when not shown suggesting that small isotopic variations recorded in cycle 10 are significant.

The supernate used for analysis of $^{143}Nd/^{144}Nd$ was dried down and dissolved sequentially in 7N HNO_3 and 15N HNO_3, drying after each acid addition. The sample was then dissolved in 4 mL 1N HNO_3, centrifuged, and the supernate was added to 250 μL cation exchange columns filled with TRU-SP resin, cleaned, and conditioned with 1N HNO_3. REE were collected using a modified method of Asmerom (1999). REE fractions were dried down and dissolved in 200 μL 0.18N HCl and were added to REE exchange columns cleaned and conditioned with 0.18N HCl. Nd was separated and collected using a modified method of Asmerom (1999). The sample solution was dried and dissolved in 1 mL 3% HNO_3 for analysis on a Thermo Neptune multi-collector inductively coupled plasma mass spectrometer (MC-ICPMS) at the University of New Mexico Radiogenic Isotope Laboratory.). Reproducibility of ε_{Nd} was determined using replicate analyses and is reported for each sample, ranging between 0.05 and 0.26 ε-units and averaging 0.11 ε-units (2σ) (Table 1, Fig. 2). Error bars of less than 0.20 ε-units are smaller than data points and therefore not shown in Fig. 2. The La Jolla Nd isotopic standard was run with each batch, obtaining a mean value of $^{143}Nd/^{144}Nd$ ratio of 0.511825 ± 4 (2σ), which is within the accepted range of values for the standard (Pier et al., 1989).

4. Results

$\delta^{18}O$ values range between 18.0 and 19.5‰. The change in $\delta^{18}O$ values across individual sampled cycles ranges between 0.5‰ and 0.9‰ (Table 1, Fig. 2). Cycles 5, 6, and 12 show progressive up-cycle increases in $\delta^{18}O$. Data for cycle 12 comes from Scott and Elrick (2004). Cycles 7 and 8 show initially increasing, then decreasing $\delta^{18}O$ trends.

ε_{Nd} values (t = 300 My; estimated age of Grey Mesa cycles) range between −10.9 and −7.4 (Table 1, Fig. 2). The change in ε_{Nd} values across individual sampled cycles ranges between 0.2 and 2.0 ε-units. Five of the eight sampled cycles are characterized by initially decreasing, then increasing ε_{Nd} values. Because only 2 samples were recovered for cycle 5, no trend is specified. Cycle 6 shows progressively decreasing ε_{Nd} values. Cycle 8 shows initially increasing, then decreasing ε_{Nd} values.

$\delta^{18}O$ vs. ε_{Nd} do not covary (Fig. 3). Systems in which the supply of continental weathering flux co-varies with $\delta^{18}O$ suggest that both isotopic systems were influenced by the same process on the same spatial or temporal scale, namely global glacial–interglacial climate changes (Vance et al., 2009). That $\delta^{18}O$ vs. ε_{Nd} do not covary suggests that these proxies were influenced by either different processes or that they are affected on a different spatial scale (e.g. global vs. regional changes).

5. Discussion

5.1. $\delta^{18}O$ trends

The systematic up-cycle increase in $\delta^{18}O$ values in 3 of 5 cycles supports the expected relationship between sea level and glacial growth and melting recorded in the Pleistocene–Holocene (e.g., Shackleton et al., 1988; Zachos et al., 2001; Lisiecki and Raymo, 2005; Raymo et al., 2006; Massari et al., 2007) and previous interpretations that these Pennsylvanian cycles were generated by glacio-eustatic sea-level change combined with some SST change (Joachimski et al., 2006; Elrick and Scott, 2010) (Fig. 2). Without the aid of independent temperature proxies such as foraminiferal Mg/Ca ratios, we cannot separate the effects of changes in glacial ice volume versus seawater temperature.

If the measured isotopic shifts were due *entirely* to SST change, then the estimated temperature change across individual cycles would range between 2 and 4 °C, applying the phosphate–water fractionation and temperature equations from Kolodny et al. (1983) and Pucéat et al. (2010). This range of temperature change would produce

Table 1
$^{143}Nd/^{144}Nd$, apparent ε_{Nd} (value at present), Sm and Nd concentrations (ppm), ε_{Nd} (t = 300 My), and $\delta^{18}O$ data for sampled intervals. t = 300 My is assumed as an approximate age for deposition of Gray Mesa cycles to determine ε_{Nd} at the time of deposition.

Cycle #	Sample[a]	$^{143}Nd/^{144}Nd$	Apparent ε_{Nd}[b]	Sm (ppm)	Nd (ppm)	ε_{Nd} @ 300 My[c]	$\delta^{18}O$ vs. SMOW
5	MS 15.25	0.51193889	−13.64	0.471	2.572	−10.37	18.66
	MS 15.75	0.51191552	−14.09	0.541	3.150	−10.56	19.15
6	MS 16.7	0.51193550	−13.70	0.273	1.723	−9.86	17.97
	MS 17.5	0.51196700	−13.09	0.702	4.732	−9.01	18.51
	MS 17.65	0.51203105	−11.84	2.543	13.910	−8.56	18.58
7	MS 18.5	0.51189999	−14.40	0.495	2.853	−10.90	18.85
	MS 19.1	0.51187610	−14.86	0.273	1.847	−10.77	19.47
	MS 19.5	0.51194919	−13.44	0.958	6.092	−9.56	18.60
8	MS 20.0	0.51197513	−12.93	2.075	12.740	−9.19	18.52
	MS 20.3	0.51201953	−12.06	0.635	3.916	−8.30	19.33
	MS 20.5	0.51206820	−11.12	1.000	6.106	−7.39	18.92
	MS 21.2	0.51201256	−12.20	0.008	0.050	−8.39	
9	MS 22.3	0.51194099	−13.60	0.728	4.028	−10.27	
	MS 22.7	0.51194725	−13.47	1.138	7.067	−9.69	
	MS 23.1	0.51192636	−13.88	0.119	0.667	−10.50	
	MS 23.6	0.51191119	−14.18	0.298	1.770	−10.56	
	MS 24.1	0.51196090	−13.21	0.208	1.231	−9.61	
	MS 24.7	0.51196808	−13.07	0.135	0.786	−9.53	
10	MS 24.9	0.51200185	−12.41	1.419	9.469	−8.36	
	MS 25.1	0.51200074	−12.43	1.051	7.055	−8.36	
	MS 25.5	0.51194909	−13.44	0.503	3.124	−9.65	
	MS 25.7	0.51194280	−13.56	0.337	2.136	−9.70	
	MS 26.0	0.51189839	−14.43	0.239	1.630	−10.31	
	MS 26.2	0.51191768	−14.05	0.138	0.913	−10.04	
	MS 26.4	0.51193553	−13.70	0.616	4.055	−9.71	
	MS 26.6	0.51192514	−13.91	0.202	1.327	−9.92	
	MS 27.2	0.51198182	−12.80	0.229	1.493	−8.84	
11	MS 28.2	0.51201351	−12.18	0.781	5.360	−8.04	
	MS 28.4	0.51202656	−11.93	1.119	7.221	−8.00	
	MS 29.1	0.51201110	−12.23	0.723	4.975	−8.08	
	MS 29.7	0.51202369	−11.98	0.434	2.934	−7.89	
	MS 30.4	0.51201959	−12.06	0.576	3.972	−7.90	
12	MS 30.5	0.51194642	−13.49	0.656	4.909	−9.07	
	MS 31.1	0.51193722	−13.67	0.898	6.314	−9.45	
	MS 31.8	0.51193345	−13.74	0.121	0.835	−9.58	
	MS 32.2	0.51190907	−14.22	0.483	3.666	−9.75	
	MS 33.7	0.51195786	−13.27	0.826	6.589	−8.65	

[a] Sample numbers represent distance (m) above underlying sequence boundary, identified by Scott and Elrick (2004).
[b] Value of ε_{Nd} at present day.
[c] ε_{Nd} during estimated time of deposition (300 My), where $^{147}Sm/^{144}Nd = Sm(ppm)/Nd(ppm) * Natural\ abundance\ of\ ^{147}Sm/^{144}Nd * atomic\ weight\ of\ Nd/Sm$, then $^{143}Nd/^{144}Nd_{(t=300\ My)} = {}^{143}Nd/^{144}Nd_{measured} - (e\lambda t - 1) * {}^{147}Sm/^{144}Nd$, and $\varepsilon_{Nd}(t = 300\ My) = (^{143}Nd/^{144}Nd_{(t=300\ My)}/^{143}Nd/^{144}Nd_{CHUR(t=300\ My)} - 1) * 10{,}000$.

only a <0.5 m thermo-eustatic sea-level change (thermal expansion/contraction of seawater; deWolde et al., 1995; Schulz and Schäfer-Neth, 1998). Such low magnitudes are unreasonable given the >50 m estimates based on facies analysis, extent and depth of subaerial exposure features, and stratal geometries (e.g. Heckel, 1977; Rygel et al., 2008). Conversely, if we assume isotopic shifts were due only to ice-volume effects, the measured 0.5–0.9‰ changes in $\delta^{18}O$ during cycle development equate to ~45–80 m glacio-eustatic changes for the sampled cycles, assuming the relationship of 0.11‰ per 10 m sea-level change (Fairbanks and Matthews, 1978).

Using the Pleistocene as an analog, we assume a combination of ice-volume and SST effects controlled the measured isotopic variations, and assume SST and ice-volume effect contributions of ~30% and ~70%, respectively (Fairbanks and Matthews, 1978; Fairbanks, 1989). Using this method, we estimate that the sampled Gray Mesa cycles were generated by >30–50 m glacio-eustatic changes accompanied by <1 °C SST changes. However, Ca/Mg ratios and $\delta^{18}O$ data from planktonic foraminifera over the past 350 kyr suggest glacial–interglacial SST changes on the order of 3–5 °C (Lea et al., 2000, 2002). If we apply 3–5 °C SST change as a minimum to sampled Pennsylvanian cycles, then the remaining isotopic shift equates to <25 m glacio-eustatic sea-level fluctuations, which would imply that SST change contributed ~70% of the total $\delta^{18}O$ value, double the estimated contribution over the last few million years (Fairbanks and Matthews, 1978; Fairbanks, 1989).

The estimated >30–50 m magnitudes record minimum values and are less than those (~60–140 m) reported by Elrick and Scott (2010). The absence of lowstand and early transgressive deposits and variability in the extent of subaerial exposure and facies changes observed at Mesa Sarca indicate that this locality did not record the full extent of sea-level rise and fall and imply that the full magnitude of glacial–interglacial isotopic shift was even larger. Much like the Pleistocene, 10^5–10^6 yr fluctuations in the volume of glacial ice during the Pennsylvanian likely contributed to the variability of sea-level change between successive cycles (Rygel et al., 2008).

It is unclear why cycles 7 and 8 show initially increasing, then decreasing $\delta^{18}O$ values, with maximum values near mid cycle (Fig. 2). Based on traditional facies analysis, which is used to interpret relative sea-level changes, these $\delta^{18}O$ versus facies relationships suggest that maximum glaciation occurred just above mid-cycle or below cycle tops, before deposition of the shallowest water facies at the cycle top. However, a more reasonable interpretation is that these cycles were generated in response to eustasy. We discuss $\delta^{18}O$ versus facies relationships using Fig. 4, which outlines the differences between relative sea-level interpreted from facies analysis versus eustatic sea-level interpreted from a theoretical understanding of the combined effects of subsidence, sea-level change, and sedimentation (Jervey, 1988; Coe and Church, 2003). Shallowing-upward facies could be generated by sedimentation rates greater than eustatic sea-level rise rates. However, this hypothesis is unlikely because the tops of cycles 7 and 8 display evidence of prolonged subaerial exposure, including pedogenic calcretes and meteoric $\delta^{13}C$ signatures, which can only form when absolute sea level falls and exposes the seafloor to meteoric waters and soil formation.

Increasing, then decreasing $\delta^{18}O$ in cycles 7 and 8 could also be generated by changes in evaporation rate and/or basin restriction, whereby increases in evaporation rate and/or basin restriction are recorded by greater $\delta^{18}O$ values. However, this hypothesis is unlikely because the greatest $\delta^{18}O$ values are recorded during the mid- to late regression when eustatic sea-level is high (Fig. 4). If evaporation rates increased during this interval, exchange with the open ocean would have also increased due to sea-level rise, dampening the effect of evaporation rate on $\delta^{18}O$ values.

5.2. Nd-isotope trends

Five of the eight sampled cycles are characterized by ε_{Nd} trends that are initially high at cycle base (maximum flooding), lowest near the mid-cycle (mid-regression), and return to high ε_{Nd} values at the cycle top (late regression; Figs. 2 and 4). These trends suggest increasing

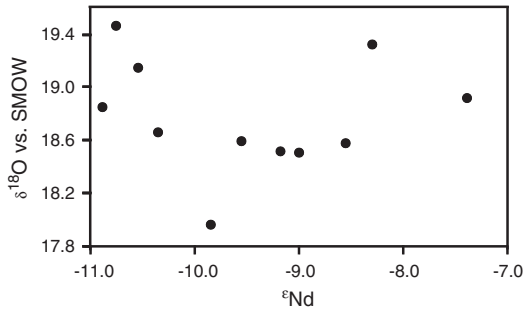

Fig. 3. ε_{Nd} vs. $\delta^{18}O$ for sampled Gray Mesa cycles. The lack of co-variance suggests that continental weathering flux (ε_{Nd}) is locally-derived. Co-variance of ε_{Nd} and $\delta^{18}O$ would suggest that changes in continental weathering flux were influenced by either the same process (i.e. glacio-eustasy and SST change) or that changes in continental weathering flux occurred on the same spatial scale (i.e. global vs. regional).

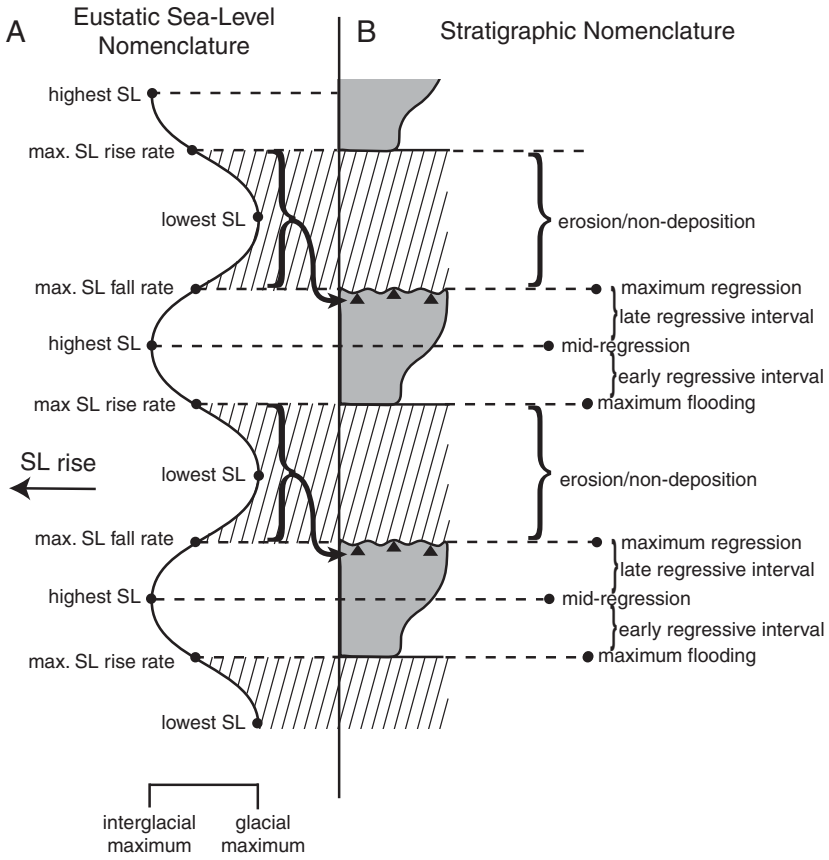

Fig. 4. A) Simplified sinusoidal eustatic sea-level (SL) curve with labeled inflection points and maximum glacial–interglacial intervals. B) Stratigraphic nomenclature used in text with schematic asymmetric cycles similar to those observed in the Gray Mesa Formation with a narrower column representing deeper water facies and a wider column representing shallower water facies. Note that no deposition/erosion occurs during the late eustatic fall, lowstand and early rise (diagonal lines) and a disconformity develops; subaerial exposure features develop at the cycle top during subaerial exposure (black triangles). During a single glacial–interglacial sea-level cycle, deposition during the initial transgression as the glaciers begin to melt is not recorded within the study area due to lack of accommodation space. Once accommodation space is created due to subsidence and rapid (maximum) SL rise rates, deposition occurs and is represented by deeper water deposits at the cycle base. SL continues to rise with additional glacial melting and reaches its highest position at the interglacial maximum (mid-regression). Because SL is rising at a slower rate after the maximum rate of SL rise inflection point (and assuming constant sedimentation rate), sediments above the maximum flooding zone reflect loss of accommodation space and is termed the early regressive interval. After the interglacial maximum, SL fall rates increase and is represented by the shallowest water deposits of the late regressive interval. The maximum regression is therefore defined in this study as the maximum regressive deposits recorded at the sampling locality.

continental weathering flux into the Lucero Basin during times of maximum flooding when sea-level was rising the fastest and until sea level reached its highest position at the interglacial maximum (mid-cycle). Subsequent increases in ε_{Nd} values suggest a reduction in continental weathering flux into the basin during initial sea-level fall. During sea-level lowstand, this inner shelf location was subaerially exposed (depositional hiatus) and no record of Nd-isotopes is available.

Four possible interpretations are explored to explain these dominant ε_{Nd} trends, each within the context of orbital-scale glacio-eustatic sea-level fluctuations. Fanton et al. (2002) interpret that ε_{Nd} increases and decreases recorded in Ordovician marine deposits represent influx from significantly different continental source areas during My-scale regression and transgression. In their scenario, the low-relief Precambrian shield (with low ε_{Nd}) was exposed during regression and submerged during transgression, which resulted in regressive marine deposits with low ε_{Nd} values and transgressive deposits with higher ε_{Nd} values. Applying this principle to the Lucero Basin, the observed ε_{Nd} trends could be produced if influx from older continental crust (with lower ε_{Nd} values) occurred during high sea level (interglacial maximum), whereas influx from younger continental crust (with higher ε_{Nd} values) reached the basin during sea-level fall (glacier growth). This scenario is not reasonable for this study because the Lucero Basin was surrounded by Precambrian uplifts (Ancestral Rocky Mountains), all with similar ages of ~1.7 Ga whose ε_{Nd} at the time of deposition of Gray Mesa cycles is ~−30 to −25 calculated from measured $^{143}Nd/^{144}Nd$ and $^{147}Sm/^{144}Nd$ reported in Bennett and DePaolo (1987); see Table 1 for calculations. Maximum exposure of these Precambrian uplifts during falling and low sea levels (glacier growth and glacial maximum) would have generated ε_{Nd} trends opposite of those observed.

A second potential explanation for the observed ε_{Nd} trends would be changes in regional marine circulation patterns. The observed ε_{Nd} trends would result from regional marine currents transporting lower ε_{Nd} values from older continental source areas flowing into the Lucero Basin during rising and high sea level (interglacials), whereas marine currents transporting higher ε_{Nd} isotope values (sourced from younger continental crust or more open-ocean waters) would flow into the Lucero Basin during falling and low sea level (early, maximum, and late glacial intervals). Because Precambrian Ancestral Rocky Mountain uplifts throughout the U.S. Southwest

have relatively uniform ε_{Nd} values (Bennett and DePaolo, 1987), it is unlikely that the Mesa Sarca ε_{Nd} trends record changes in influx from significantly different continental crust source areas and it is unlikely that the same marine circulation patterns would have occurred for six successive cycles formed during variable magnitude sea-level changes.

Instead, we explore two alternative mechanisms that can explain changes in continental weathering flux on orbital timescales. In a scenario in which eolian transport dominated continental influx into the Lucero Basin, rising sea levels (early interglacials or cycle bases) are characterized by low eolian influx due to low wind intensities and/or greater humidity/wetter climate, and resultant high ε_{Nd} values. This would be followed by increasing eolian influx due to increasing winds/aridity during highest sea-levels (interglacial maximums or mid-cycles), resulting in low ε_{Nd} values. During subsequent sea-level fall (early glacial), eolian input would decline with decreasing wind intensity and/or aridity and a return to higher ε_{Nd} values. While a few studies from tropical and temperate Pacific Ocean cores report increased eolian input during Pleistocene or Holocene interglacial intervals (Rea et al., 1986; Hovan et al., 1991), the majority of findings from these studies suggest that glacial intervals are characterized by drier climates and greater wind intensities, whereas interglacial intervals have wetter climates and lower wind intensities globally (e.g. van Zeist, 1967; Janecek and Rea, 1983; Wasson et al., 1984; Rea et al., 1991; Nanson et al., 1992; Wang, 1993; Rea, 1994; Rincón-Martínez et al., 2010). Without a process-oriented model explaining windier/more arid conditions during interglacial intervals, it is not reasonable to expect that wind behavior during glacial Pennsylvanian intervals opposed the dominant Pleistocene regime.

We suggest that the observed ε_{Nd} trends were likely controlled by orbitally-driven changes in continental weathering rates and/or fluvial sediment influx. Accordingly, the observed trends would develop if fluvial influx and/or chemical weathering rates were low (resulting in higher ε_{Nd} values), increasing during maximum sea-level rise rates (early interglacial), and were greatest, signaled by lower ε_{Nd} values, during sea-level highs (interglacial maxima); fluvial influx and/or weathering rates would then decrease (rising ε_{Nd} values) during the subsequent fall in sea level (early glacial) (Fig. 4). We suggest that the systematic changes in fluvial influx and/or chemical weathering rates were controlled by orbitally-forced changes in paleotropical precipitation and/or air temperature, in which increases in precipitation and/or air temperature resulted in increased fluvial influx and/or chemical weathering rates and decreases in precipitation and/or air temperature resulted in decreased fluvial influx and/or weathering rates.

Many modern watersheds are shown to be 'weathering limited', characterized by thinner soils with readily available unaltered minerals, such that weathering flux is limited by mineralogy (susceptibility to chemical weathering), precipitation, soil–water pH, and temperature (Stallard and Edmond, 1981, 1983, 1987; Kump et al., 2000). Global continental chemical weathering rates are shown to increase with rises in temperature and precipitation demonstrated by increases in fluvial discharge cation concentrations, Ca, Mg, K, HCO_3^-, and H_4SiO_4 (e.g., Bluth and Kump, 1994; White and Blum, 1995; Berner et al., 1998; Kump et al., 2000; Frank, 2002; West et al., 2005; Schmidt et al., 2006; Gislason et al., 2009; McKay et al., 2009; Kuwahara et al., 2010; Williams et al., 2010). Indeed, positive coupling of chemical weathering rates with precipitation and temperature is also demonstrated over orbitally-driven glacial–interglacial cycles (e.g. Burton and Vance, 2000; Piotrowski et al., 2005; Bokhorst et al., 2009; Kuwahara et al., 2010). Because air temperature often co-varies with precipitation, evaporation rates, and vegetation cover, it is difficult to separate the effects of temperature and precipitation on chemical weathering rates (Kump et al., 2000). To separate the effects of temperature and precipitation, White and Blum (1995) fit an Arrhenius-type equation to SiO_2 and Na fluxes. Although plots of weathering fluxes versus temperature correlate reasonably well, they significantly underestimate chemical weathering rates, suggesting that precipitation dominates chemical weathering rates and that precipitation and temperature are positively coupled.

The relationship between drier glacials and wetter interglacials is consistent with results from paleoequatorial regions in the Late Pennsylvanian (Soreghan, 1994; Rankey, 1997) and Pleistocene–Holocene (e.g. van Zeist, 1967; Janecek and Rea, 1983; Wasson et al., 1984; Rea et al., 1991; Nanson et al., 1992; Wang, 1993; Rea, 1994; Rincón-Martínez et al., 2010). In particular, planktonic foraminifera from the Bay of Bengal demonstrate cyclic variations in ε_{Nd} on glacial–interglacial timescales over the past 150 kyr due to variations in continental weathering flux (Burton and Vance, 2000). Each of these examples is characterized by cooler, drier climates during glacial maxima with a relatively low flux of fluvially-derived material (reflected by higher ε_{Nd}) and warmer, wetter interglacial intervals, in which flux of fluvially-derived material increases (reflected by lower ε_{Nd}) (Burton and Vance, 2000; Naimo et al., 2005; Kettner and Syvitski, 2009; Lewis et al., 2009).

Vance et al. (2009) suggest that the products of chemical weathering on glacial–interglacial timescales are moderated by post-glacial weathering pulses (fine-grained physical weathering products produced by subglacial grinding underneath continental glaciers; Bell and Laine, 1985; Anderson, 2007) released during glacial melting and retreat. Post-glacial weathering pulses are more likely to be observed in ferromanganese nodules in post-glacial lakes (Vance et al., 2009), deep-ocean ferromanganese crusts (Reynolds et al., 1999; Piotrowski et al., 2005), and marine sediments along high-latitude continental shelves (Scher et al., 2011). Low-latitude shelf localities are less likely to record post-glacial pulses because global transport of REEs such as Nd and Sm occur via large-scale ocean circulation (i.e. modern transport from the Labrador Surface Water current to the North Atlantic Deep Water current and then the Antarctic Bottom Water current; e.g., Burton et al., 1997; Piotrowski et al., 2005; Scher and Martin, 2006; Via and Thomas, 2006). Due to their low mobility, REEs will likely be scavenged by particulates before a high-latitude post-glacial weathering pulse can be recorded in marine sediments accumulating on a low-latitude shelf. In addition, the lack of co-variance between $\delta^{18}O$ and ε_{Nd} supports the assumption that ε_{Nd} values are locally-derived (Fig. 3).

One of the eight sampled cycles (cycle 6) records a progressive increase in ε_{Nd} values from cycle base to top and one cycle (cycle 8) shows an initial increase to peak ε_{Nd} values in the middle of the cycle followed by a decrease in values within the cycle cap (Fig. 2). These variable trends may be due to fluctuations in sedimentation rate, thus recording an incomplete eustatic sea-level curve over cycle development (Fig. 4). Long-term variations in the magnitude of Pliocene through Pleistocene orbital-scale climate forcing are a possible explanation for variations in continental weathering flux, if changes in the magnitude of climatic forcing control the proclivity of chemical versus mechanical weathering. Differences in ε_{Nd} between the acid soluble (AS) and acid insoluble (AIS) fraction of samples may elucidate whether ε_{Nd} values were incorporated into the crystal structure of carbonate minerals (suggesting chemical weathering dominated) or whether ε_{Nd} is a primary signature of the detrital component (suggesting mechanical weathering dominated). Such a test may also explain why sediments deposited during the interglacial maximum do not necessarily possess the greatest detrital (AIS) fraction.

It is important to note that if our hypothesis of increased continental weathering flux during sea-level highstands (interglacials) is due to increased precipitation (and as a result, increased fluvial flux), then it opposes traditional sequence stratigraphic interpretations, where sea-level controls shoreline and fluvial base-level positions and by implication, the flux of continentally-derived sediment into the marine basin (e.g. Van Wagoner et al., 1988; Coe and Church, 2003). In the traditional sequence stratigraphic model, sea-level fall/

lowstands are characterized by fluvial incision and increased fluvial transport to the marine basin, which would be recorded by an up-cycle increase in $\varepsilon_{Nd.}$ In contrast, our hypothesized model suggests that increased fluvial incision and/or transport of physical weathering products (solids) and dissolved chemical weathering products (dissolved load) (shown by increased ε_{Nd}) coincide with intervals of sea-level rise and highstand (interglacial), followed by decreased fluvial incision and/or flux (shown by decreasing ε_{Nd}) during sea-level fall/lowstand (glaciation) (Fig. 4). Increased fluvial incision is indeed more likely to occur during maximum regression due to lowering of fluvial base level, however the type of weathering (physical versus chemical), the mechanism of transport (fluvial versus eolian) and weathering rates to generate transportable particles is dominated by local/regional, climatically controlled changes in precipitation and/or air temperature.

Results from this study highlight how orbital to suborbital variations in ε_{Nd} and $\delta^{18}O$ within marine strata can detect the response of continental weathering flux to orbitally-forced climate change and eliminates potential miscorrelations between geographically separated marine and coeval non-marine successions. These results demonstrate that Middle Pennsylvanian paleotropical continental weathering flux is generally in-phase with glacio-eustatic sea-level change and glacial growth/melting, and suggest that local/regional paleotropical continental weathering may be dependent upon climatically controlled changes in fluvial flux due to fluctuations in precipitation and/or air temperature. These results highlight a promising new technique utilizing nearshore marine successions to evaluate regional continental weathering flux and climate change within the context of global sea-level and glacial–interglacial cycles.

6. Conclusions

1) $\delta^{18}O$ trends across targeted orbital-scale subtidal cycles support previous interpretations that these cycles formed in response to glacio-eustasy with magnitudes of between 30 and 50 m combined with ~1 °C SST changes.
2) The majority of cycles sampled for ε_{Nd} analysis display trends indicating maximum continental weathering flux during interglacial maxima (sea-level highstands) when local paleotropical precipitation rates and/or paleotemperatures were the highest, facilitating maximum weathering rates and/or fluvial transport of weathered solutes to the study area. During lower sea-level stands (early and late glacial stages), continental weathering flux decreased, suggesting drier and/or cooler paleotropical climates. Because these cycles were deposited at an inner shelf location, no record is available for lowest sea-level positions (glacial maximum).
3) Our hypothesis of increased continental weathering influx during sea-level highstands (interglacials) is in contrast to traditional sequence stratigraphic interpretations and suggests that climatically controlled precipitation and/or air temperature fluctuations influenced continental weathering flux more than sea-level controlled shoreline/base line position in this paleotropical location.

Acknowledgments

This work was supported by NSF proposal EAR-0920830 and RAC funding from the University of New Mexico. Many thanks to Viorel Atudorei, Victor Polyak, Stephanie Yurchyk, Andrew Yuhas, and Zach Wallace for their assistance in the lab and in conducting fieldwork. We would also like to thank two anonymous reviewers for their insightful comments and suggestions.

References

Algeo, T., Wilson, J.L., and Lohmann, K.C., 1991. Eustatic and tectonic controls on cyclic sediment accumulation patterns in Lower-Middle Pennsylvanian strata of the Orogrande Basin, New Mexico, New Mexico Geological Society Guidebook 42, 203–212.
Amzy, K., Veizer, J., Bassett, M.G., Copper, P., 1998. Oxygen and carbon isotopic composition of Silurian brachiopods: implications for coeval seawater and glaciations. GSA Bulletin 110, 1499–1512.
Anderson, R.Y., 1982. A long geoclimatic record from the Permian. Journal of Geophysical Research 87, 7285–7294.
Anderson, S.P., 2007. Biogeochemistry of glacial landscape systems. Annual Review of Earth and Planetary Sciences 35, 375–399.
Arens, N.C., Jahren, A.H., 2000. Carbon isotope excursion in atmospheric CO_2 at the Cretaceous–Tertiary boundary: evidence from terrestrial sediments. Palaios 15, 314–322.
Arthur, M.A., Bottjer, D.J., Dean, W.E., Fischer, A.G., Hattin, D.E., Kauffman, E.G., Pratt, L.M., SCholle, P.A., 1986. Rhythmic bedding in Upper Cretaceous pelagic carbonate sequences; varying sedimentary response to climatic forcing. Geology 14, 153–156.
Asmerom, Y., 1999. Th–U fractionation and mantle structure. Earth and Planetary Science Letters 166, 163–175.
Banner, J.L., 2004. Radiogenic Isotopes: systematics and applications to earth surface processes and chemical stratigraphy. Earth-Science Reviews 65, 141–194.
Bassett, D., MacLeod, K.G., Miller, J.F., Ethington, R.L., 2007. Oxygen isotopic composition of biogenic phosphate and the temperature of Early Ordovician seawater. Palaios 22, 98–103.
Bell, M., Laine, E.P., 1985. Erosion of the Laurentide region of North America by glacial and glaciofluvial processes. Quaternary Research 23, 154–174.
Bennett, V.C., DePaolo, D.J., 1987. Proterozoic crustal history of the Western United States as determined by neodymium isotopic mapping. Geological Society of America Bulletin 99, 674–685.
Berner, R.A., Rao, J.-L., Chang, S., O'Brien, R., Keller, C.K., 1998. Seasonal variability of adsorption and exchange equilibria in soil waters. Aquatic Geochemistry 4, 273–290.
Bluth, G.J.S., Kump, L.R., 1994. Lithologic and climatologic controls of river chemistry. Geochimica et Cosmochimica Acta 58, 2341–2359.
Bokhorst, M.P., Beets, C.J., Markovic, S.B., Gerasimenko, N.P., Matviishina, Z.N., Frechen, M., 2009. Pedo-chemical climate proxies in late Pleistocene Serbian–Ukrainian loess sequences. Quaternary International 198, 113–123.
Bryant, J.D., Koch, P.L., Froelich, P.N., Showers, W.J., Genna, B.J., 1996. Oxygen isotope partitioning between phosphate and carbonate in mammalian apatite. Geochimica et Cosmochimica Acta 60, 5145–5148.
Burton, K.W., Vance, D., 2000. Glacial–interglacial variations in the neodymium isotope composition of seawater in the Bay of Bengal recorded by planktonic Foraminifera. Earth and Planetary Science Letters 176, 425–441.
Burton, K.W., Ling, H.F., O'Nions, R.K., 1997. Closure of the central American Isthmus and its effect on deep water formation in the North Atlantic. Nature 386, 382–385.
Caputo, M.V., Crowell, J.C., 1985. Migration of glacial centers across Gondwana during the Paleozoic era. Geological Society of America Bulletin 96, 1020–1036.
Coe, A.L., Church, K.D., 2003. In: Coe, Angela L. (Ed.), The sedimentary record of sea-level change. Cambridge University Press, pp. 57–98.
Crowell, J.C., 1999. Pre-Mesozoic ice ages: their bearing on understanding the climate system. Geological Society of America Memoir 192, 1–106.
Culver, S.J., Farrell, K.M., Mallinson, D.J., Willard, D.A., Horton, B.P., Riggs, S.R., Theiler, E.R., Wehmiller, J.F., Parham, P., Snyder, S.W., Hillier, C., 2011. Micropaleontologic record of Quaternary paleoenvironments in the central Albemarle Embayment, North Carolina, U.S.A. Palaeogeography, Palaeoclimatology, Palaeoecology 305, 227–249.
deWolde, J.R., Bintania, R., Oerlemans, J., 1995. On thermal expansion over the last hundred years. Journal of Climate 8, 2881–2891.
Dickinson, W.R., Lawton, T.F., 2003. Sequential intercontinental suturing as the ultimate control for Pennsylvanian Ancestral Rocky Mountains deformation. Geology 31, 609–612.
Elrick, M., Scott, L.A., 2010. Carbon and oxygen isotope evidence for high-frequency (104–105 yr) and My-scale glacioeustasy in Middle Pennsylvanian cyclic carbonates (Gray Mesa Formation), central New Mexico. Palaeogeography, Palaeoclimatology, Palaeoecology 285, 307–320.
Elrick, M., Berkyova, S., Klapper, G., Sharp, Z., Joachimski, M., Fryda, J., 2009. Stratigraphic and oxygen isotope evidence for My-scale glaciations driving eustasy in the Early–Middle Devonian greenhouse world. Palaeogeography, Palaeoclimatology, Palaeoecology 276, 170–181.
Emiliani, C., 1955. Pleistocene temperatures. Journal of Geology 63, 538–578.
Emiliani, C., 1966. Isotopic paleotemperatures. Science 154, 851–857.
Epstein, S., Buschbaum, R., Lowenstam, H.A., Urey, H.C., 1953. Revised carbonate–water isotopic temperature scale. Geological Society of America Bulletin 64, 1315–1326.
Fairbanks, F.G., 1989. A 17,000-year glacio-eustatic sea level record; influence of glacial melting rates on the Younger Drays event and deep-ocean circulation. Nature 342, 637–642.
Fairbanks, F.G., Matthews, R.K., 1978. The marine oxygen isotope record in Pleistocene coral, Barbados, West Indies. Quaternary Research 10, 181–196.
Fanton, K., Holmden, C., Nowlan, G., Haidl, F., 2002. $^{143}Nd/^{144}Nd$ and Sm/Nd stratigraphy of Upper Ordovician epeiric sea carbonates. Geochimica et Cosmochimica Acta 66, 241–255.
Fielding, C.R., Frank, T.D., Birgenheier, L.P., Rygel, M.C., Jones, A.T., Roberts, J., 2008. Stratigraphic imprint of the Late Palaeozoic Ice Age in eastern Australia: a record of alternating glacial and-non-glacial climate regime. Geological Society of London Journal 165, 129–140.
Frakes, L.A., Francis, J.E., 1988. A guide to Phanerozoic cold polar climates from high-latitude ice-rafting in the Cretaceous. Nature 333, 547–549.

Frank, M., 2002. Radiogenic isotopes: tracers of past ocean circulation and erosional input. Reviews of Geophysics 40, 1–38.

Gale, A.S., Hardenbol, J., Hathaway, B., 2002. Global correlation of the Cenomanian (Upper Cretaceous) sequences: evidence for Milankovitch control on sea level. Geology 30, 291–294.

Gislason, S.R., Oelkers, E.H., Eiriksdottir, J., Torsannder, P., Oskarsson, N., 2009. Direct evidence of the feedback between climate and weathering. Earth and Planetary Science Letters 277, 213–222.

Goldhammer, R.K., 1987. Platform carbonate cycles, Middle Triassic of northern Italy; the interplay of local tectonics and global eustasy, Dissertation, Johns Hopkins University, Baltimore, Maryland, 548 pp.

Goldhammer, R.K., Elmore, R.D., 1984. Paleosols capping regressive carbonate cycles in the Pennsylvanian Black Prince Limestone, Arizona. Journal of Sedimentary Petrology 54, 1124–1137.

Goldstein, S.J., Jacobsen, S.B., 1987. The Nd and Sr isotopic systematic of river-water dissolved material; implications for the sources of Nd and Sr in seawater. Chemical Geology 66, 245–272.

Heckel, P.H., 1977. Origin of phosphatic black shale facies in Pennsylvanian cyclothems of mid-continent North America. American Association of Petroleum Geologists Bulletin 61, 1045–1068.

Heckel, P.H., 1994. Evaluation of evidence for glacio-eustatic control over marine Pennsylvanian cyclothems in North America and consideration of possible tectonic effects. In: Dennison, J.M., Ettensohn, F.R. (Eds.), Tectonic and eustatic controls on sedimentary cycles: SEPM (Society for Sedimentary Geology) Concepts in Sedimentology and Paleontology, 4, pp. 65–87.

Hovan, S.A., Rea, D.K., Pisias, N.G., 1991. Late Pleistocene continental climate and oceanic variability recorded in Northwest Pacific sediments. Paleoceanography 6, 349–370.

Iacumin, P., Bocherens, H., Mariotti, A., Longinelli, A., 1996. Oxygen isotope analysis of co-existing carbonate and phosphate in biogenic apatite: a way to monitor diagenetic alteration of bone phosphate? Earth and Planetary Science Letters 142, 1–6.

Isbell, J.L., Miller, M.F., Wolfe, K.L., Lenaker, P.A., 2003. Timing of the late Paleozoic glaciation in Gondwana: was glaciation responsible for the development of Northern Hemisphere cyclothems? In: Chan, M.A., Archer, A.W. (Eds.), Extreme depositional environments: mega end-members in geologic time: GSA Spec. Paper, 370, pp. 5–24.

Jahren, A.H., Amundson, R., Kendall, C., Wigand, P., 2001. Paleoclimatic reconstruction using the correlation in delta (super 18) O of hackberry carbonate and environmental water, North America. Quaternary Research 56, 252–263.

Janecek, T.R., Rea, D.K., 1983. Eolian deposition in the Northeast Pacific Ocean; Cenozoic history of atmospheric circulation. Geological Society of America Bulletin 94, 730–738.

Jervey, M.T., 1988. Quantitative geological modeling of siliciclastic rock sequences and their seismic expressions. In: Wilgus, C.K., Hastings, B.S., Kendall, C.G.St.C., Posamentier, H.W., Ross, C.A., Van Wagoner, J.C. (Eds.), Sea-Level Changes; An Integrated Approach: Society of Economic Paleontologists and Mineralogists: Special Publication, 42, pp. 47–69.

Joachimski, M.M., Geldern, R., Breisig, S., Bruggisch, W., Day, J., 2004. Oxygen isotope evolution of biogenic calcite and apatite during the Middle and Late Devonian. International Journal Earth Science 93, 542–553.

Joachimski, M.M., von Bitter, P.H., Buggisch, W., 2006. Constraints on Pennsylvanian glacioeustatic sea-level changes using oxygen isotopes on conodont apatite. Geology 34, 277–280.

Karlstrom, K.E., Amato, J.M., Williams, M.L., Heizler, M., Shaw, C.A., 2004. Proterozoic tectonic evolution of the New Mexico region; a synthesis. Special Publication New Mexico Geological Society 11, 1–34.

Kelly, V.C., Wood, G.H., 1946. Lucero uplift, Valencia, Socorro, and Bernalillo counties. U.S.G.S, New Mexico. Oil and Gas Inventory Preliminary Map 47.

Kettner, A.J., Syvitski, J.P.M., 2009. Fluvial responses to environmental perturbations in the Northern Mediterranean since the Last Glacial Maximum. Quaternary Science Reviews 28, 2386–2397.

Kluth, C.F., Coney, P.J., 1981. Plate tectonics of the Ancestral Rocky Mountains. Geology 9, 10–15.

Kolodny, Y., Luz, B., Navon, O., 1983. Oxygen isotope variations in phosphate of biogenic apatites; I fish bone apatite; rechecking the rules of the game. Earth and Planetary Science Letters 64, 398–404.

Kues, B.S., Giles, K.A., 2004. The Late Paleozoic Rocky Mountains system in New Mexico. Special Publication New Mexico Geological Society 11, 95–136.

Kump, L.R., Brantley, S.L., Arthur, M.A., 2000. Chemical weathering, atmospheric CO_2, and climate. Annual Reviews in Earth and Planetary Science 28, 611–667.

Kuwahara, Y., Masudome, Y., Paudel, M.R., Fujii, R., Hayashi, T., Mampuku, M., Sakai, H., 2010. Controlling weathering and erosion intensity on the southern slope of the central Himalaya by the Indian summer monsoon during the last glacial. Global and Planetary Change 71, 73–84.

Laurin, J., Meyers, S.R., Sageman, B.B., Waltham, D., 2005. Phase-lagged amplitude modulation of hemipelagic cycles: a potential tool for recognition and analysis of sea-level change. Geology 33, 569–572.

Lea, D.W., Pak, D.K., Spero, H.J., 2000. Climate impact of Late Quaternary equatorial Pacific sea surface temperature variations. Science 289, 1719–1724.

Lea, D.W., Martin, P.A., Pak, D.K., Spero, H.J., 2002. Reconstructing a 350 ky history of sea level using planktonic Mg/Ca and oxygen isotope records from a Cocos Ridge core. Quaternary Science Reviews 21, 283–293.

Lewis, C.J., McDonald, E.V., Sancho, C., Pena, J.L., Rhodes, E.J., 2009. Climatic implications of correlated upper Pleistocene glacial and fluvial deposits of the Cinca and Gallego Rivers (NE Spain) based on OSL dating and soil stratigraphy. Global and Planetary Change 67, 141–152.

Lisiecki, L.E., Raymo, M.E., 2005. A Pliocene–Pleistocene stack of 57 globally distributed benthic $\delta^{18}O$ records. Paleoceanography 20, 1003.

Lozovsky, V.R., Yarshenko, O.P., 1994. The Permian/Triassic boundary in the continental series of the Moscow syneclise: recent achievements. Permophiles 24, 54–59.

MacLeod, K.G., Martin, E.E., Blair, S.W., 2008. Nd isotopic excursion across Cretaceous ocean anoxic event 2 (Cenomanian–Turonian) in the tropical North Atlantic. Geology 36, 811–814.

Martin, J.L., 1971. Stratigraphic analysis of Pennsylvanian strat in the Lucero region of west-central New Mexico: Unpublished Ph.D. dissertation, University of New Mexico, 196 pp.

Martin, E.E., Macdougall, J.D., 1995. Sr and Nd isotopes at the Permain/Triassic boundary: a record of climate change. Chemical Geology 125, 73–99.

Massari, F., Capraro, L., Rio, D., 2007. Climatic modulation of timing of systems-tract development with respect to sea-level changes (Middle Pleistocene of Crotone, Calabria, southern Italy). Journal of Sedimentary Research 77, 461–468.

McKay, C.P., Molaro, J.L., Marinova, M.M., 2009. High frequency rock temperature data from hyper-arid desert environments in the Atacama and the Antarctic dry valleys and implications for rock weathering. Geomorphology 110, 182–187.

McLennan, S.M., 1989. Rare earth elements in sedimentary rocks: influence of provenance and sedimentary processes. In: Lipin, B.R., McKay, G.A. (Eds.), Geochemistry and Mineralogy of Rare Earth Elements: Reviews in Mineralogy, 21, pp. 169–200.

Miller, K.B., McCahon, T.J., West, R.R., 1996. Lower Permian (Wolfcampian) paleosolbearing cycles of the U.S. Midcontinent: evidence of climatic cyclicity. Journal of Sedimentary Research 66, 71–84.

Mundil, R., Zuehlke, R., Bechstaedt, T., Peterhaensel, A., Egenhoff, S.O., 2003. Cyclicities in Triassic platform carbonates: synchronizing radio-isotopic and orbital clocks. Terra Nova 15, 81–87.

Naimo, D., Adamo, P., Imperato, M., Stanzione, D., 2005. Mineralogy and geochemistry of a marine sequence, Gulf of Salerno, Italy. Quaternary International 140–141, 53–63.

Nanson, G.C., Price, D.M., Short, S.A., 1992. Wetting and drying of Australia over the past 300 ka. Geology 20, 791–794.

O'Neil, J.R., Roe, L.J., Reinhard, E., Blacke, R.E., 1994. A rapid and precise method of oxygen isotope analysis of biogenic phosphate. Israel Journal of Earth Science 43, 203–212.

Olson, P.E., Kent, D.V., 1999. Long-period Milankovitch cycles from the Late Triassic and Early Jurassic of eastern North America and their implications for the calibration of the Early Mesozoic time-scale and the long-term behavior of the planets. Philosophical Transactions of the Royal Society of London 357, 1761–1786.

Pier, J.G., Podosek, F.A., Luhr, J.A., Brannon, J.C., Ara-Gomez, J.J., 1989. Spinel–iherzolite-bearing Quaternary volcanic centers in San Luis Potosi, Mexico, 2. Sr and Nd isotope systematics. Journal of Geophysical Research 94, 7941–7951.

Piotrowski, A.M., Goldstein, S.L., Hemming, S.R., Fairbanks, R.G., 2005. Temporal relationships of carbon cycling and ocean circulation at glacial boundaries. Science 307, 1933–1938.

Pucéat, E., Lécuyer, C., Reisberg, L., 2005. Neodymium isotope evolution of NW Tethyan upper ocean waters throughout the Cretaceous. Earth and Planetary Science Letters 236, 706–720.

Pucéat, E., Joachimski, M.M., Bouilloux, A., Monna, F., Bonin, A., Motreuil, S., Moriniere, P., Henard, S., Mourin, J., Dera, G., Quesne, D., 2010. Revised phosphate–water fractionation equation reassessing paleotemperatures derived from biogenic apatite. Earth and Planetary Science Letters 298, 135–142.

Rankey, E.C., 1997. Relations between relative changes in sea level and climate shifts: Pennsylvanian–Permian mixed carbonate–siliciclastic strata, western United States. Geological Society of America Bulletin 109, 1089–1100.

Raymo, M.E., Lisiecki, L.E., Nisancioglu, K.H., 2006. Plio–Pleistocene ice volume, Antarctic climate, and the global $\delta^{18}O$ record. Science 313, 492–495.

Rea, D.K., 1994. The paleoclimatic record provided by eolian deposition in the deep sea; the geologic history of wind. Reviews of Geophysics 32, 159–195.

Rea, D.K., Chambers, L.W., Chuey, J.M., Janecek, T.R., Leinen, M., Pisias, N.G., 1986. A 420,000-year record of cyclicity in oceanic and atmospheric processes from the eastern Equatorial Pacific. Paleoceanography 1, 577–586.

Rea, D.K., Pisias, N.G., Newberry, T., 1991. Late Pleistocene paleoclimatology of the central Equatorial Pacific; flux patterns of biogenic sediments. Paleoceanography 6, 227–244.

Reynolds, B.C., Frank, M., O'Nions, R.K., 1999. Nd- and Pb-isotope time series from Atlantic ferromanganese crusts: implications for changes in provenance and paleocirculation over the last 8 Myr. Earth and Planetary Science Letters 173, 381–396.

Rincón-Martínez, D., Lamy, F., Contreras, S., Leduc, G., Bard, E., Saukel, C., Blanz, T., Mackensen, A., Tiedemann, R., 2010. More humid interglacials in Ecuador during the past 500 kyr linked to latitudinal shifts of the equatorial front and the Intertropical Convergence Zone in the eastern tropical Pacific. Paleoceanography 25, 2210.

Rygel, M.C., Fielding, C.R., Frank, T.D., Birgenheier, L.P., 2008. The magnitude of Late Paleozoic glacioeustatic fluctuations: a synthesis. Journal of Sedimentary Research 78, 500–511.

Scher, H.D., Martin, E.E., 2006. Timing and climatic consequences of the opening of Drake Passage. Science 312, 428–430.

Scher, H.D., Bohaty, S.M., Zachos, J.C., Delaney, M.L., 2011. Two-stepping into the icehouse; east Antarctic weathering during progressive ice-sheet expansion at the Eocene–Oligocene transition. Geology 39, 383–386.

Schmidt, R., Kamenik, C., Tessadri, R., Koining, K.A., 2006. Climatic changes from 12,000 to 4,000 years ago in the Austrian central Alps tracked by sedimentological and biological proxies of a lake sediment core. Journal of Paleolimnology 35, 491–505.

Schulz, M., Schäfer-Neth, C., 1998. Translating Milankovitch climate forcing into eustatic fluctuations via thermal deep water expansion: a conceptual link. Terra Nova 9, 228–231.

Scotese, C.R., 2001. Quicktime Computer Animations. PALEOMAP Project Department of Geology, University of Texas at Arlington, Arlington, Texas.

Scotese, C.R., Galonka, J., 1992. PALEOMAP Paleogeographic Atlas, PALEOMAP Progress Report No. 20. Department of Geology, University of Texas at Arlington, Arlington, Texas. 34 pp.
Scott, L.A., Elrick, M., 2004. Cycle and sequence stratigraphy of Middle Pennsylvanian (Desmoinsian) strata of the Lucero Basin, central New Mexico. In: Lucas, S.G., Zeigler, K.E. (Eds.), New Mexico Museum of Natural History and Science Bulletin, pp. 31–41.
Shackleton, N.J., Opdyke, N.D., 1973. Oxygen isotope and palaeomagnetic stratigraphy of Equatorial Pacific Core V28-238: oxygen isotope temperatures and ice volumes on a 105 and 106 year scale. Quaternary Research 3, 39–55.
Shackleton, N.J., Imbrie, J., Pisias, N.G., 1988. The evolution of oceanic oxygen-isotope variability in North Atlantic over the past three million years. Philosphical Transactions of the Royal Society of London, Series B: Biological Sciences 318, 1191.
Shirey, S.B., 1991. The Rb–Sr, Sm–Nd and Re–Os isotopic systems; a summary and comparison of their applications to the cosmochronology and geochronology of igneous rocks. Applications of Radiogenic Isotope Systems to Problems in Geology: Short Course Handbook, 19, pp. 103–166.
Shishkin, M.A., Ochev, V.G., 1993. The Permo-Triassic transition and the Early Triassic history of the Euramerican tetrapod fauna. Bulletin—New Mexico Museum of Natural History and Science. .
Soreghan, G.S., 1994. Stratigraphic responses to geologic processes: Late Pennsylvanian eustasy and tectonics in the Pedrogosa and Orogrande basins, Ancestral Rocky Mountains. Geological Society of America Bulletin 106, 1195–1211.
Soreghan, G.S., Giles, K.A., 1999. Amplitudes of Late Pennsylvanian glacioeustasy. Geology 27, 255–258.
Stallard, R.F., Edmond, J.M., 1981. Geochemistry of the Amazon 1. Precipitation chemistry and the marine contribution to the dissolved load at the time of peak discharge. Journal of Geophysical Research 86, 9844–9985.
Stallard, R.F., Edmond, J.M., 1983. Geochemistry of the Amazon 2. The influence of geology and weathering environment on the dissolved load. Journal of Geophysical Research 88, 9671–9688.
Stallard, R.F., Edmond, J.M., 1987. Geochemistry of the Amazon 3.Weathering chemistry and limits to dissolved inputs. Journal of Geophysical Research 92, 8293–8302.
Sweet, A.G., Harris, W.C., 1988. Mechanical and chemical techniques for separating microfossils from rock, sediment, and residue matrix. Special Publication, Paleontological Society 4, 70–86.
Thomas, D.J., 2004. Evidence for deep-water production in the North Pacific Ocean during the early Cenozoic warm interval. Nature 430, 65–68.
Van Wagoner, J.C., Posamentier, H.W., Mitchum, R.M., Vail, P.R., Sarg, J.F., Loutit, T.S., Hardenbol, J., 1988. An overview of the fundamentals of sequence stratigraphy and key definitions. In: Wilgus, C.K., Hastings, B.S., Kendall, C.G.St.C., Posamentier, H.W., Ross, C.A., Van Wagoner, J.C. (Eds.), Sea Level Changes: An Integrated Approach: SEPM, Special Publication, 42, pp. 39–45.
van Zeist, W., 1967. Late Quaternary vegetation history of western Iran. Review of Palaeobotany and Palynology 2, 301–311.
Vance, D., Teagle, D.A.H., Foster, G.L., 2009. Variable Quaternary chemical weathering fluxes and imbalances in marine geochemical budgets. Nature 458, 493–496.
Veevers, J.M., Powell, C. McA, 1987. Late Paleozoic glacial episodes in Gondwanaland reflected in transgressive–regressive depositional sequences in Euramerica. Geological Society of America Bulletin 98, 475–487.
Veizer, J., Ala, D., Amzy, K., Bruckschen, P., Buhl, D., Bruhn, F., Carden, G.A.F., Diener, A., Ebneth, S., Godderis, Y., Jasper, T., Korte, C., Pawellek, F., Podlaha, O.G., Strauss, H., 1999. $^{87}Sr/^{86}Sr$, $\delta^{13}C$, and $\delta^{18}O$ evolution of Phanerozoic seawater. Chemical Geology 161, 59–88.
Via, R.K., Thomas, D.J., 2006. Evolution of Atlantic thermohaline circulation: Early Oligocene onset of deep-water production in the North Atlantic. Geology 34, 441–444.
Wang, Y., 1993. Lacustrine carbonate chemical sedimentation and climatic-environmental evolution—a case study of Qinghai lake and Daihai lake, China. Oceanologia et Limnologia Sinica 24, 31–36.
Wasson, R.J., Smith, G.I., Agrawal, D.P., 1984. Late Quaternary sediments, minerals, and inferred geochemical history of Didwana Lake, Thar Desert, India. Palaeogeography, Palaeoclimatology, Palaeoecology 46, 345–372.
Wengerd, S.A., 1959. Regional geology as related to the petroleum potential of the Lucero region, west–central New Mexico. New Mexico Geological Society Guidebook, 10th Field Conference, pp. 121–134.
Wenzel, B., Lecuyer, C., Joachimski, M., 2000. Comparing oxygen isotope records of Silurian calcite and phosphate-d^{18}O compositions of brachiopods and conodonts. Geochimica et Cosmochimica Acta 64, 1859–1872.
West, A.J., Galy, A., Bickle, M., 2005. Tectonic and climatic controls on silicate weathering. Earth and Planetary Science Letters 235, 211–228.
White, A.F., Blum, A.E., 1995. Effects of climate on chemical weathering in watersheds. Geochimica et Cosmochimica Acta 59, 1729–1747.
Wiberg, T.L., Smith, G.A., 1994. Pennsylvanian glacio-eustasy recorded in a carbonate ramp succession, Ancestral Rocky Mountains, New Mexico. Canadian Society of Petroleum Geologists 17, 545–556.
Williams, J.Z., Bandstra, J.Z., Pollard, D., Brantley, S.L., 2010. The temperature dependence of feldspar dissolution determined using a coupled weathering-climate model for Holocene-ages loess soils. Geoderma 156, 11–19.
Ye, H., Royden, L., Burchfiel, C., Schuepbacj, M., 1996. Late Paleozoic deformation of interior North America: the greater Ancestral Rocky Mountains. American Association of Petroleum Geologists Bulletin 80, 1397–1432.
Zachos, J., Pagani, M., Sloan, L., Thomas, E., Billups, K., 2001. Trends, rhythms, and aberrations in global climate 65 Ma to present. Science 292, 686–693.